Revisiting MnP_4 as negative electrode for Li-ion batteries: mechanism and performance

Julien Fullenwarth,[a] Bernard Fraisse,[a] Nicolas Dupré,[b] Lorenzo Stievano, [a,c] Laure Monconduit[a,c, *]

[a] *ICGM, Univ. Montpellier, CNRS, ENSCM, 34293 Montpellier Cedex 5, France*

[b]*Institut des Matériaux Jean Rouxel (IMN), CNRS UMR 6502, Univ. Nantes, 44322 Cedex 3 Nantes, France*

[c]*Réseau sur le Stockage Electrochimique de l'Energie (RS2E), FR CNRS 3459, France*

Supplementary Information

Synthesis: Stoichiometric amounts of manganese metal (Mn Alfa Aesar, 325 mesh, 99.3%) and red phosphorous (P Alfa Aesar, 100 mesh, 99%) was inserted in stainless steel vial with 6 balls 10mm diameter (4g each ball). The volume of the used vial is 45mL and the ratio powder balls 1:24. Fritsch premium pulverisette 7 was used for 150 cycles (15 minutes of milling + 10 minutes of rest). Powder morphology and particle size were investigated by scanning electron microscopy (SEM) with a Hitachi S-4500 microscope. Micrometric size particles were indeed obtained as revealed by SEM analysis (Figure SI 1).

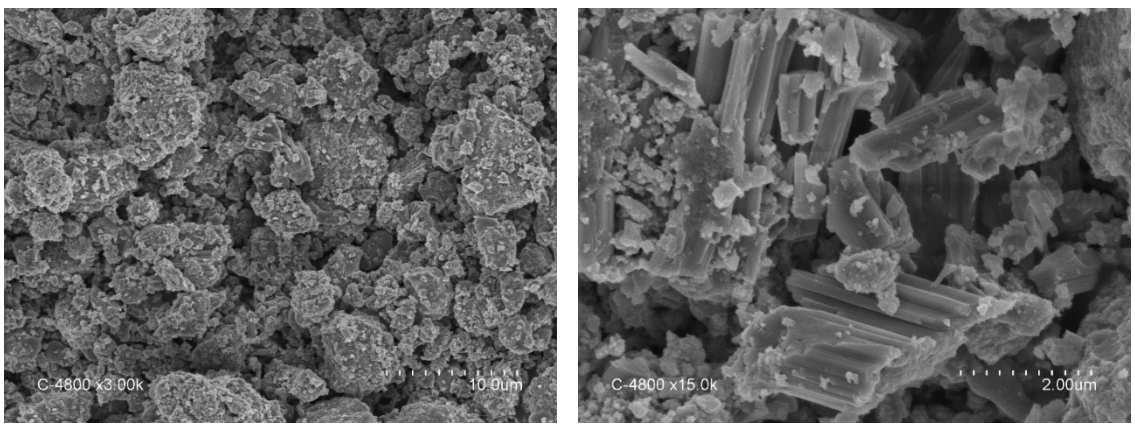

Figure SI 1: SEM of MnP_4 powder sample

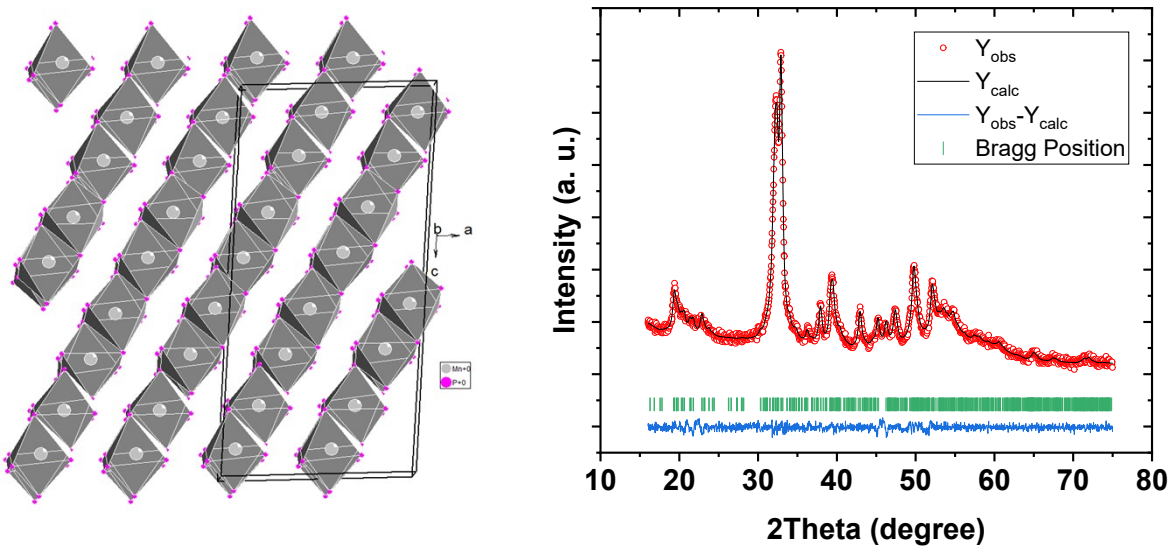

Figure SI 2: Crystallographic structure and X-ray profil matching refinement of MnP_4 powder sample (obtained by ball milling). The XRD pattern was recorded on a Panalitical Empyrean diffractometer equipped with a Cu Kα radiation in the Bragg-Brentano configuration. The refined (Fullprof software) cell parameters in triclinic space group *P-1* are $a = 16.320(1)$ Å, $b = 5.8499(5)$ Å, $c = 5.1053(6)$ Å, $\alpha = 115.659(8)°$, $\beta = 95.138(1)°$, $\gamma = 89.214(5)°$, in good agreement with ICSD 16416.

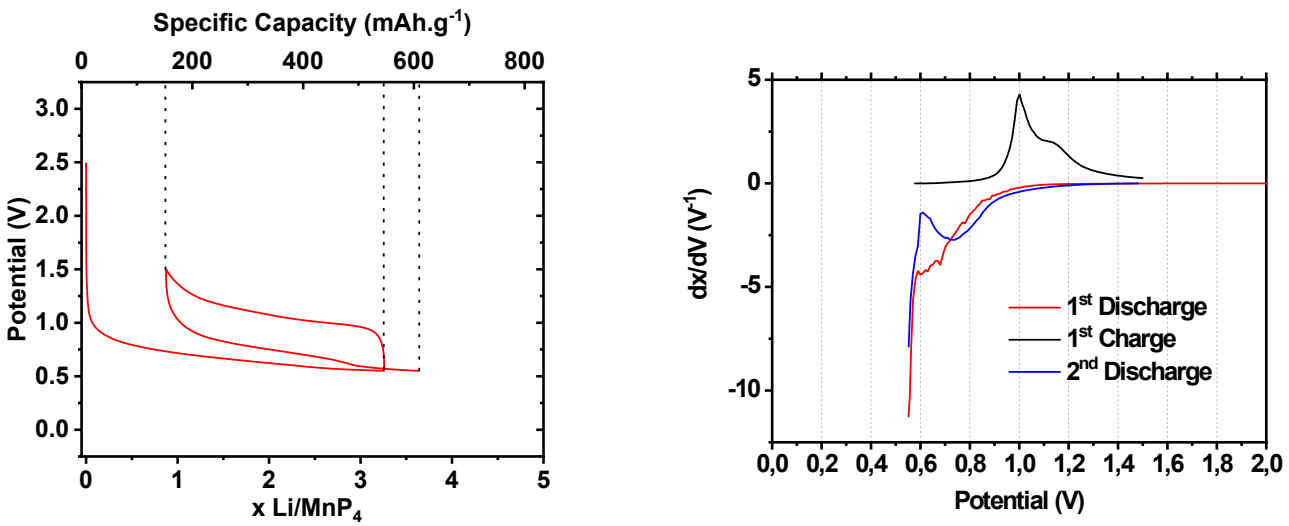

(a) (b)

Figure SI 3: galvanostatic curves and associated derivative of MnP_4 vs Li, (a) in the 0.5-1.5V potential window and (b) in the limited 0.4-1.5V potential window (recorded at C/2).

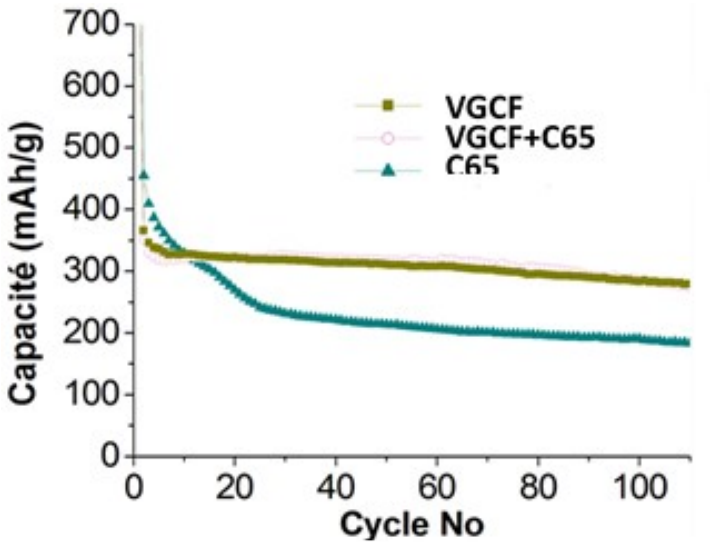

Figure SI 4: electrochemical measurement of a CMC-based electrode containing only C65 and VGCF (1:1). The initial coulombic efficiency (ICE) of this electrode is approximately 43%.

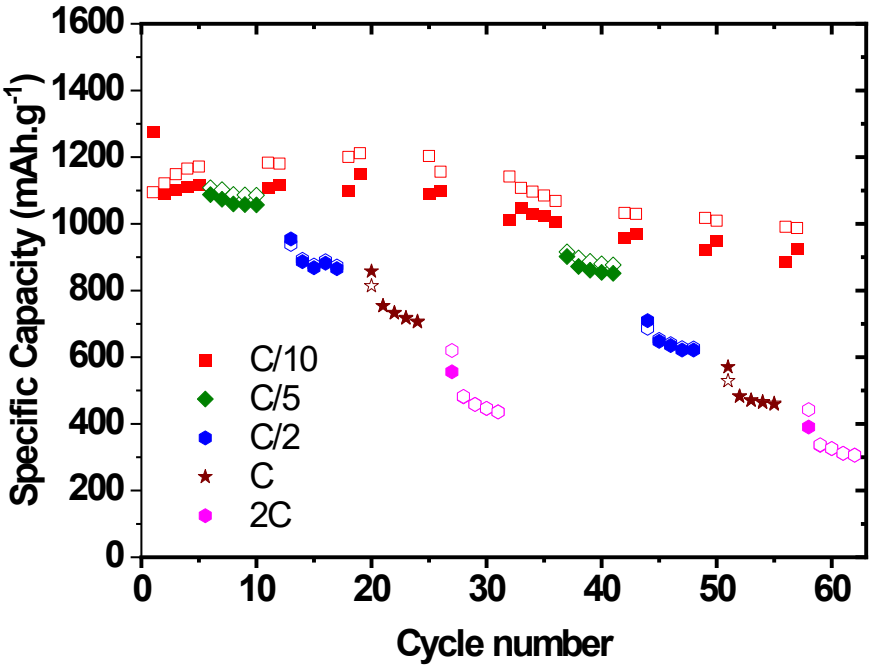

(a)

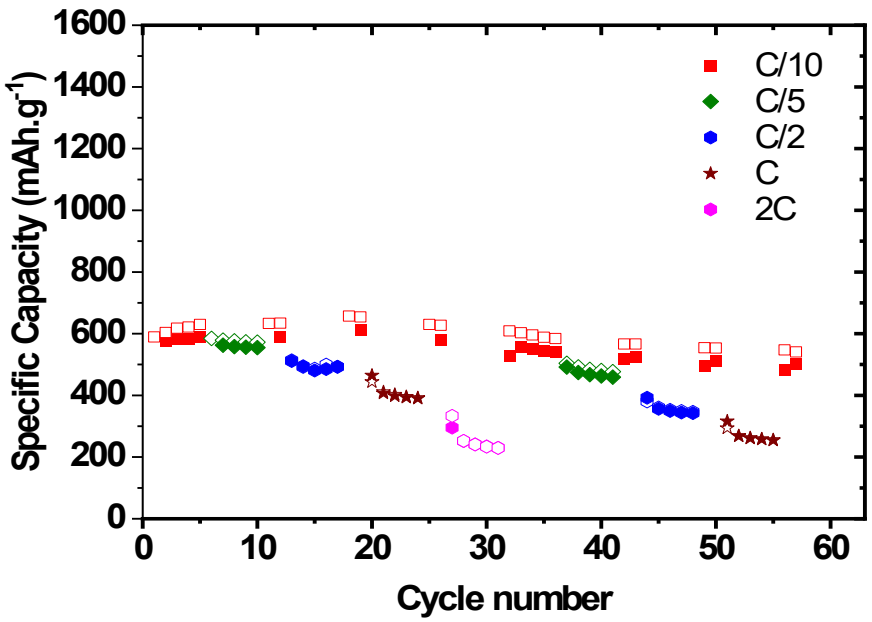

(b)

Figure SI 5: Rate capability for the full (a) and limited 0.55 - 1.5 V potential window (b).

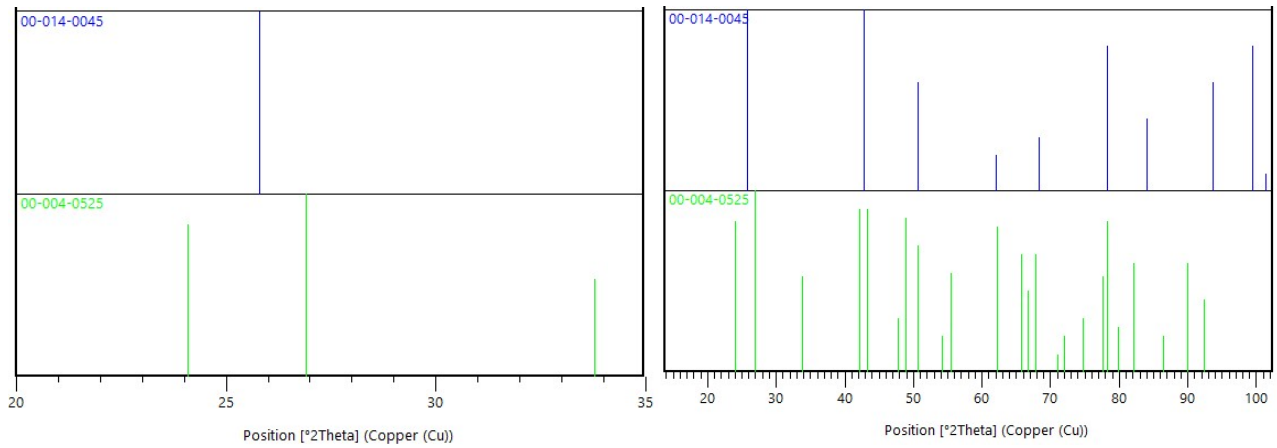

Figure SI 6: Theoretical XRD patterns of Li_7MnP_4 (cubic, Fm-3m, 00-014-0045) in blue and Li_3P (hexagonal, $P6_3/mmc$, 00-004-0525) in green.

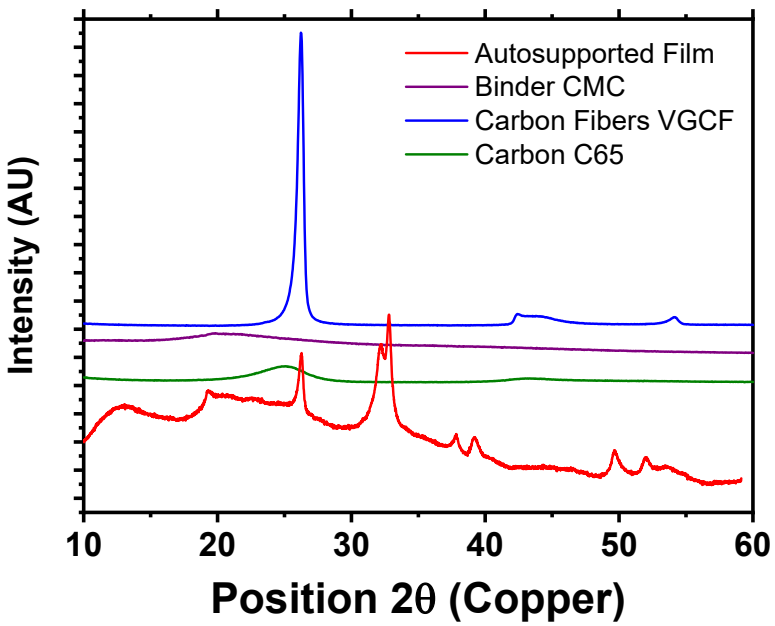

Figure SI 7: X-ray characterization of carbon additives (C65/VGCF), used in the MnP_4 electrode formulation**.** The XRD patterns were recorded on a Panalitical Empyrean diffractometer equipped with a Cu Kα radiation in the Bragg-Brentano configuration.

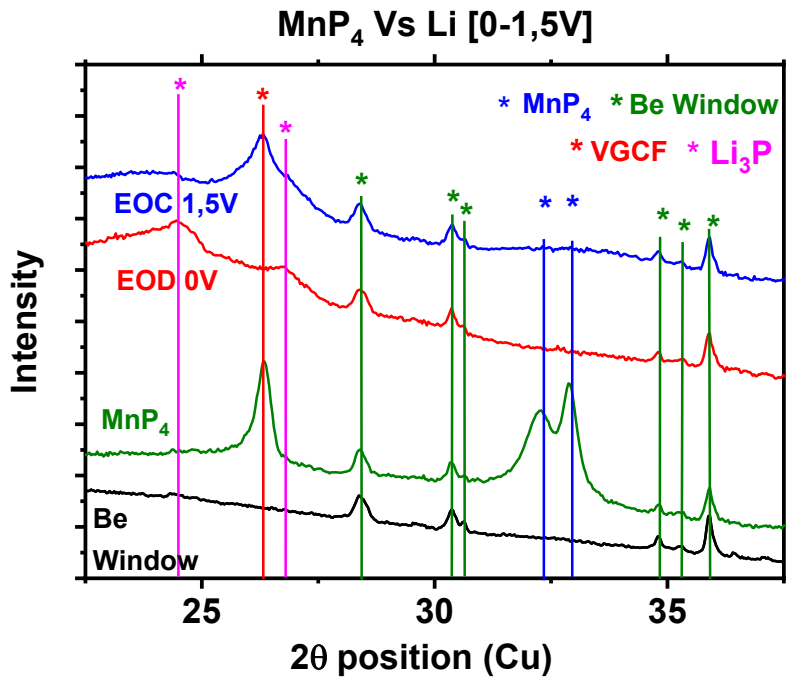

(a)

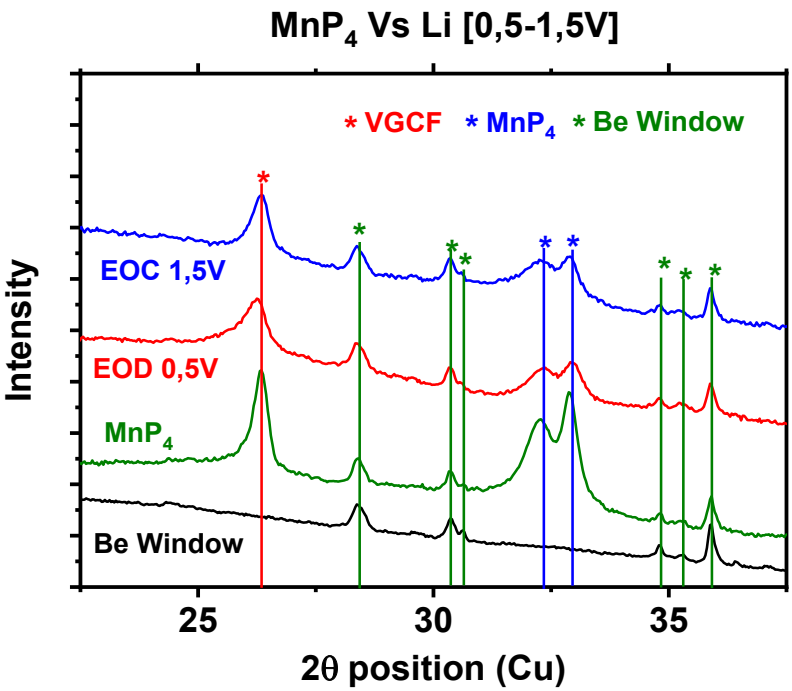

(b)

Figure SI 8: Ex situ X-ray characterization (Cu) of MnP_4/Li battery for the full (a) and limited 0.55-1.5V potential window (b).

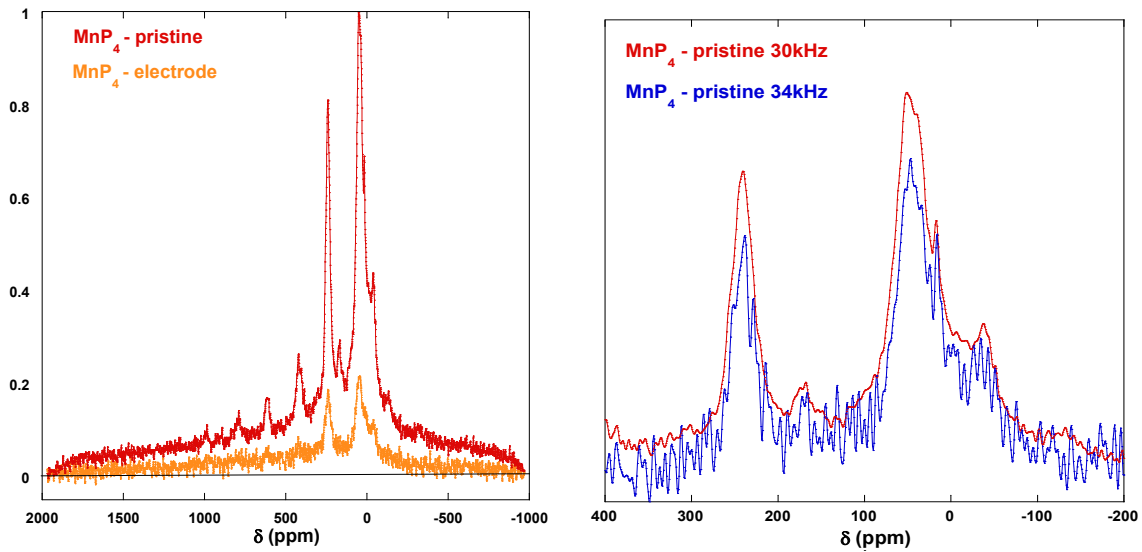

Figure SI 9: a) Normalized ^{31}P NMR spectra of a pristine MnP_4 and a MnP_4 electrode. Spectra were normalized with respect to the mass of sample, number of scans and taking into account the presence of 15% of carbon additive in the electrode b) ^{31}P MAS NMR spectra of pristine MnP_4 at different spinning speeds: 30 kHz (red) and 34kHz (blue)

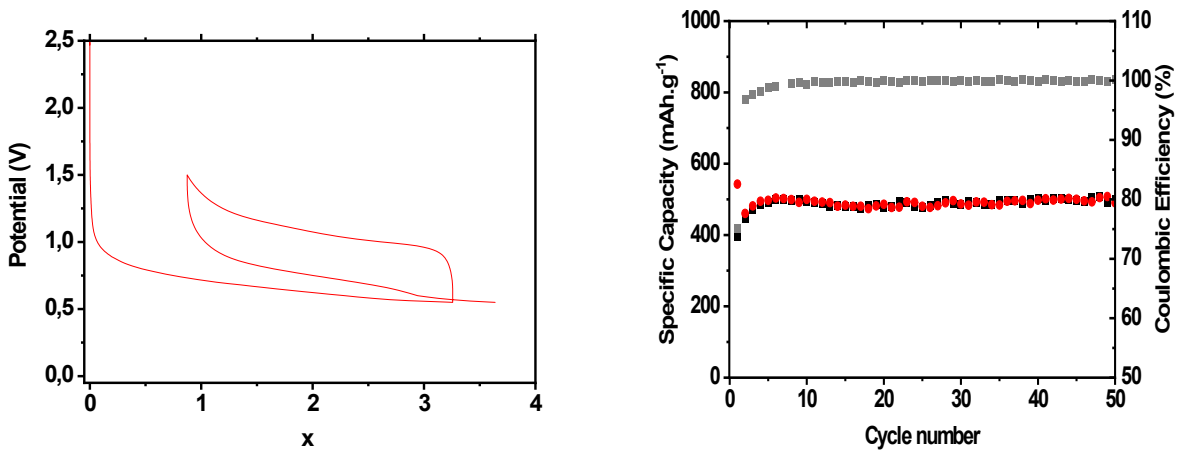

Figure SI 10: a) galvanostatic curve and b) capacity retention measured at C/2 rate of the MnP_4/Li cell measured in the 0.55-1.5V potential window.

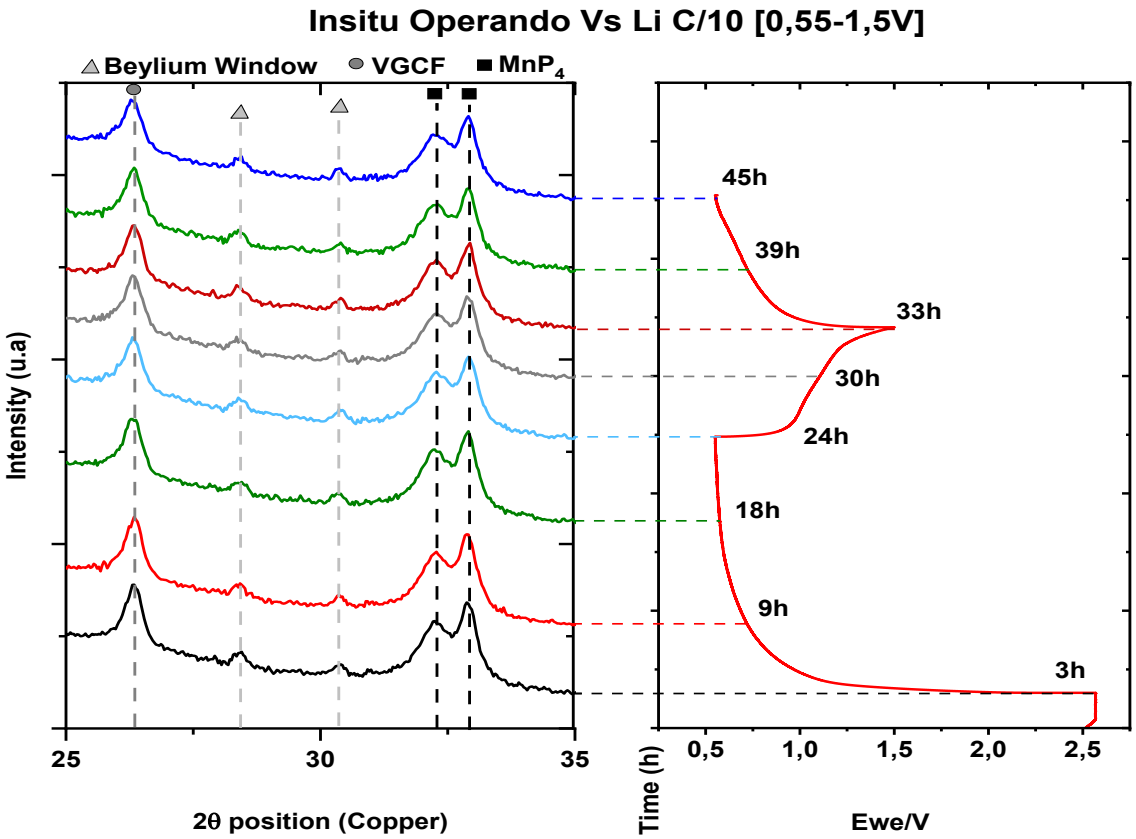

Figure SI 11: XRD operando of MnP_4/Li cell during the first cycles at x (rate) in the [0.55 – 1.5V] potential window and associated galvanostatic curve. Operando XRD measurements were carried out using an electrochemical cell equipped with a 250 µm-thick beryllium window in reflection mode

X-ray absorption spectroscopy

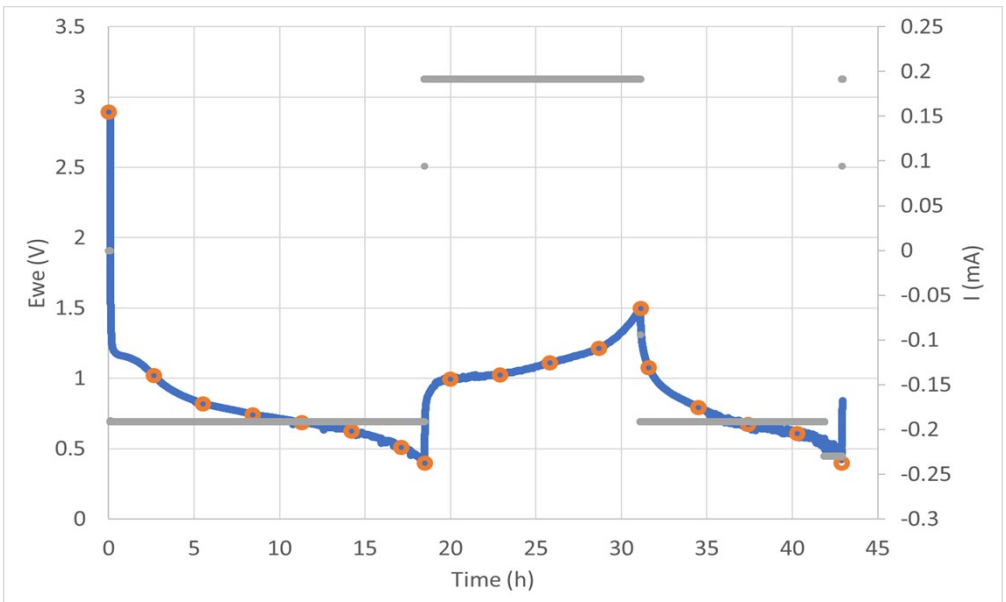

Fig SI 12: Galvanostatic discharge-charge curve measured during the *operando* XAS experiment with the low voltage cut-off at 0.4 V, and correspondence with the measured spectra.

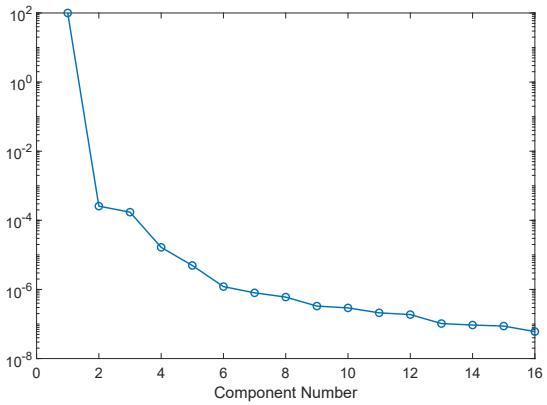

(a)

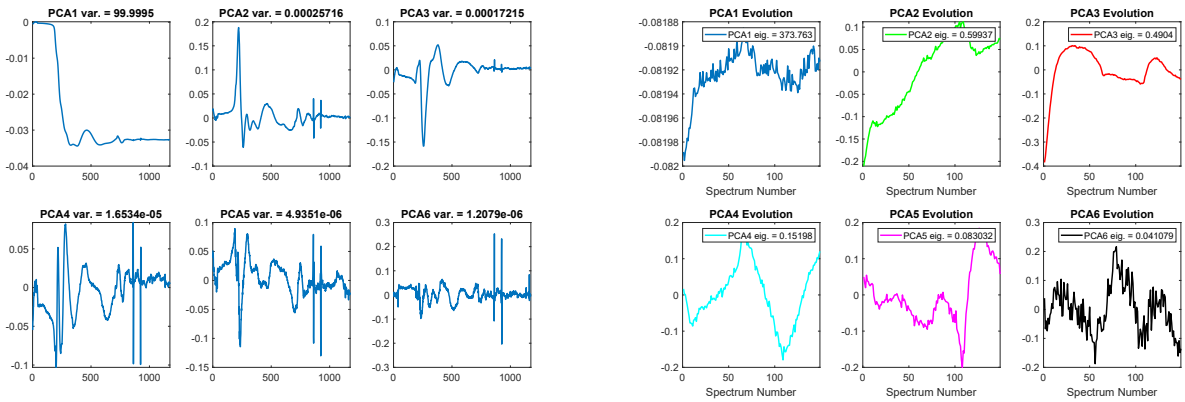

(b) (c)

Fig SI 13: Results of the PCA of the dataset collected during the *operando* XAS experiment with the low voltage cut-off at 0.4 V: **(a)** variance plot; **(b)** principal components; **(c)** evolution of the scores.

The fitting of the EXAFS portion of the five MCR-ALS components obtained from the analysis of the XAS dataset collected during the *operando* XAS experiment with the low voltage cut-off at 0.4 V was performed starting from the structure of MnP_4, with the following cell parameters

- Symmetry: triclinic, space group #2 ($P\bar{1}$)
  - a = 16.347
  - b = 5.847
  - c = 5.108
  - α = 115.66
  - β = 95. 15
  - γ = 89.21

In order to simplify the fitting treatment, the different neighbour shells were defined by averaging the three different Mn sites, which led to the following shells:

- 1st Mn-P shell: 6 P @ 2.25 Å
- 2nd Mn-Mn shell: 1 Mn @ 2.95 Å

– 3rd Mn-Mn shell: 1 Mn @ 3.70 Å
– 4th Mn-P shell: 10 P @ 3.85 Å

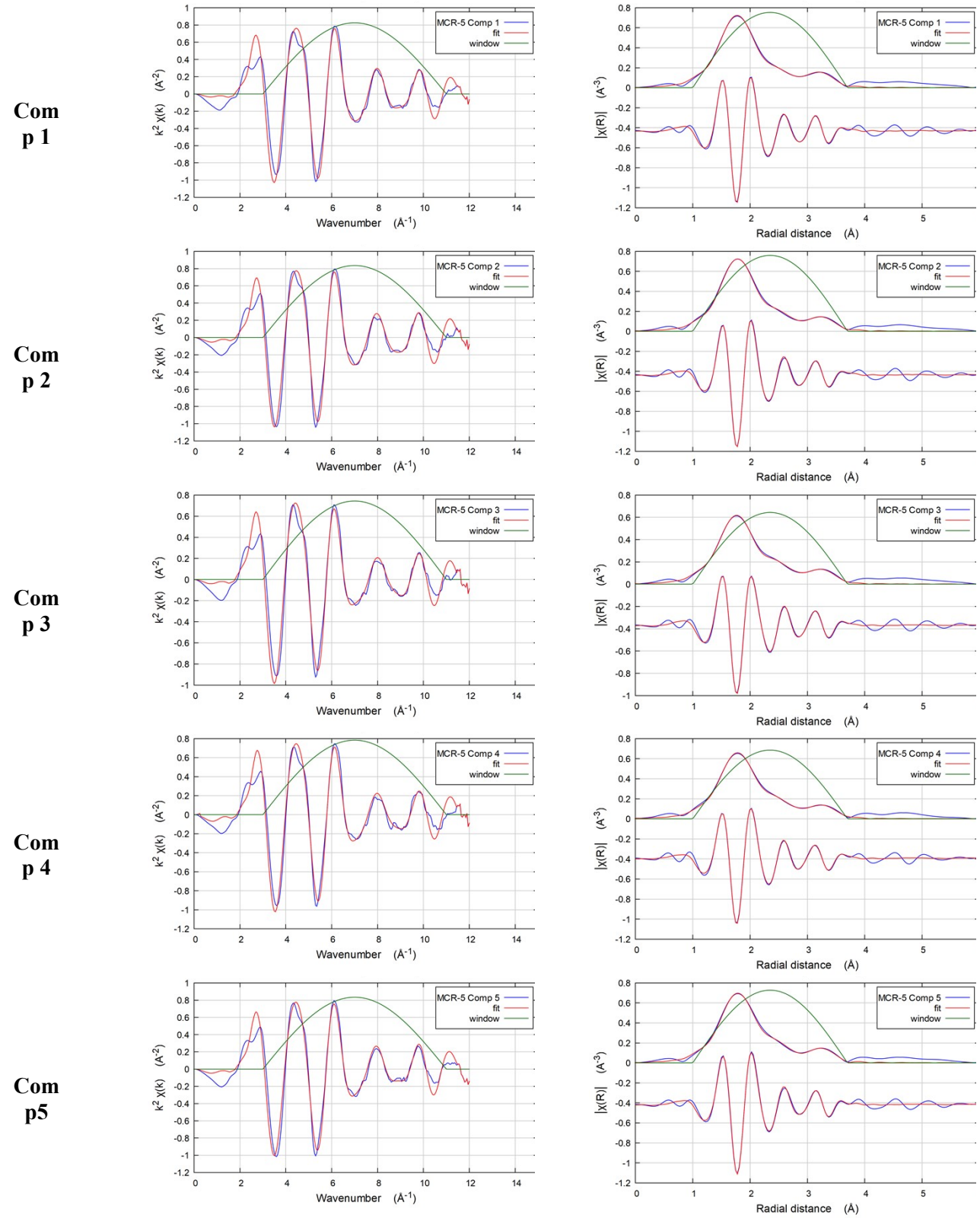

Fig SI 14. Fits of the EXAFS portion of the 5 MCR-ALS pure components obtained by the analysis of the dataset collected during the experiment with the low voltage cut-off at 0.4 V: EXAFS signal (left) and Fourier Transform (right).

Table S1. Fitting parameters of the EXAFS signal of the 5 MCR-ALS pure components obtained by the analysis of the dataset collected during the experiment with the low voltage cut-off at 0.4 V.

Component	Shell	S_0^2	N	R (theory)	R (fitted)	σ^2
Comp 1	Mn-P	0.50	6	2.25	2.281(7)	0.0074(3)
	Mn-Mn		1	2.95	2.69(1)	0.0021(8)
	Mn-Mn		1	3.75	3.63(2)	0.003(2)
	Mn-P		10	3.90	3.92(3)	0.025(5)
Comp 2	Mn-P	0.50	6	2.25	2.291(7)	0.0074(3)
	Mn-Mn		1	2.95	2.69(1)	0.0014(8)
	Mn-Mn		1	3.75	3.64(2)	0.003(2)
	Mn-P		10	3.90	3.98(3)	0.026(5)
Comp 3	Mn-P	0.50	6	2.25	2.289(8)	0.0091(3)
	Mn-Mn		1	2.95	2.70(1)	0.0018(8)
	Mn-Mn		1	3.75	3.64(3)	0.005(2)
	Mn-P		10	3.90	3.91(3)	0.028(5)
Comp 4	Mn-P	0.50	6	2.25	2.292(7)	0.0085(3)
	Mn-Mn		1	2.95	2.70(1)	0.0017(8)
	Mn-Mn		1	3.75	3.64(2)	0.005(3)
	Mn-P		10	3.90	3.92(3)	0.027(5)
Comp 5	Mn-P	0.50	6	2.25	2.295(8)	0.0078(4)
	Mn-Mn		1	2.95	2.70(1)	0.0013(9)
	Mn-Mn		1	3.75	3.65(2)	0.002(2)
	Mn-P		10	3.90	3.94(4)	0.030(7)

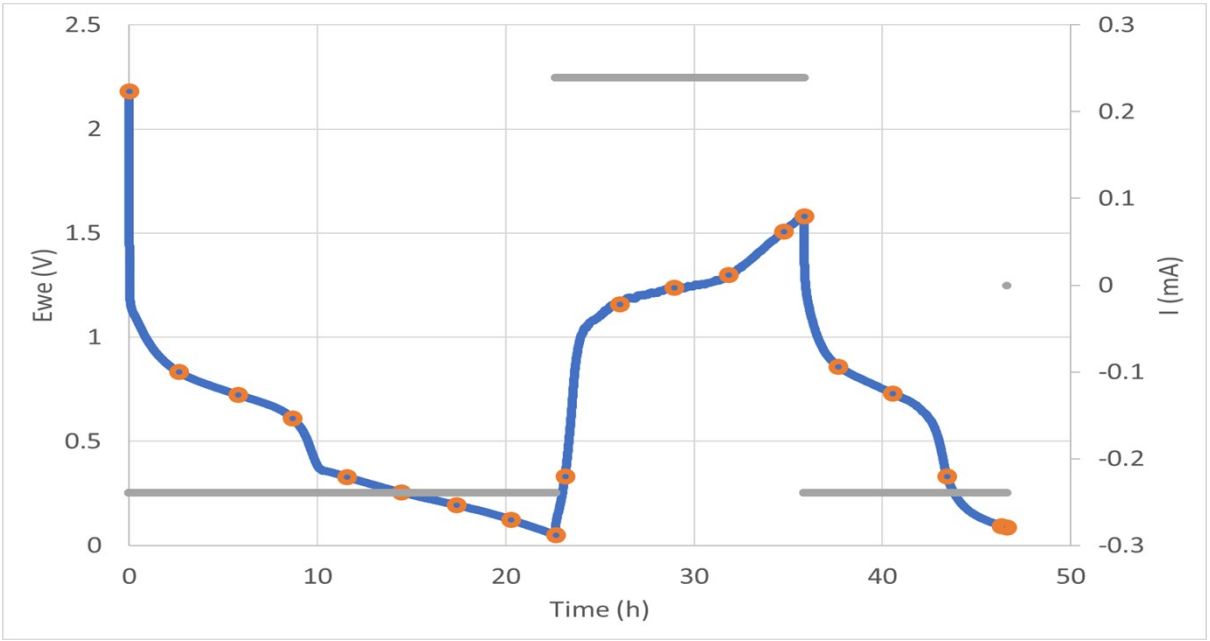

Fig SI 15. Galvanostatic discharge-charge curve measured during the *operando* XAS experiment with the low voltage cut-off at 0.01 V, and correspondence with the measured spectra.

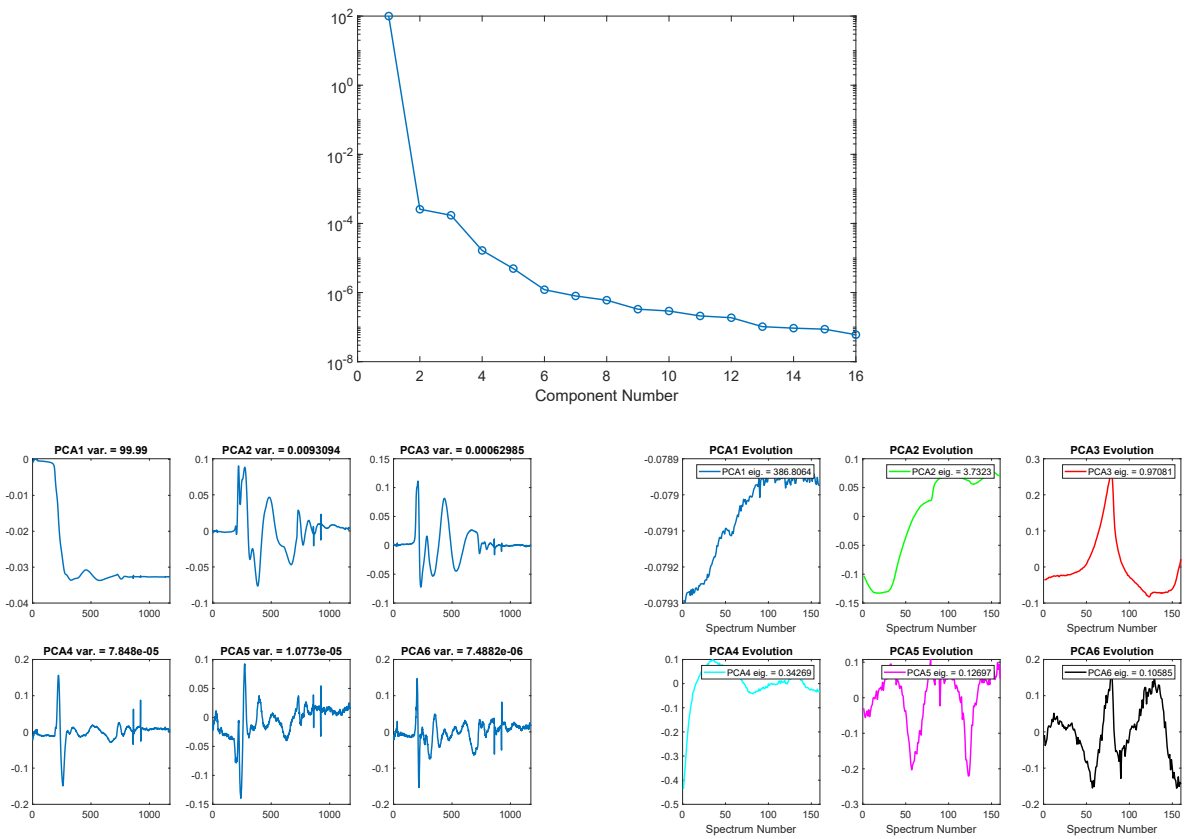

Fig SI 16. Results of the PCA of the dataset collected during the *operando* XAS experiment with the low voltage cut-off at 0.01 V: **(a)** variance plot; **(b)** principal components; **(c)** evolution of the scores.

Comp 1

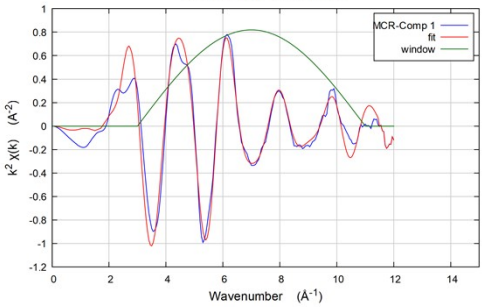

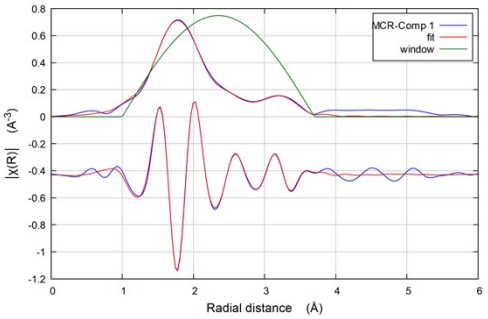

Comp 2

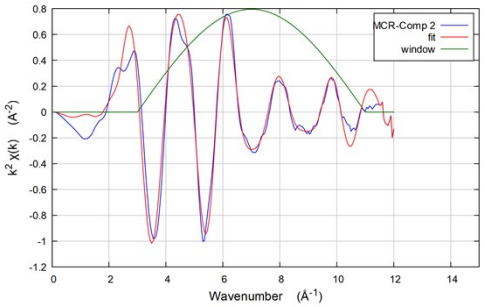

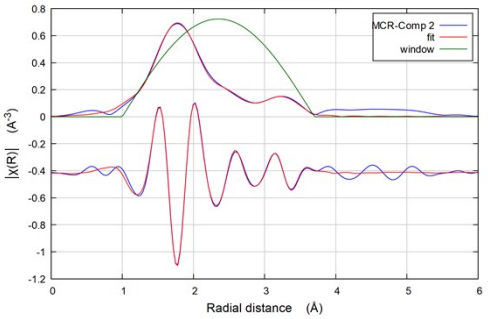

Comp 3

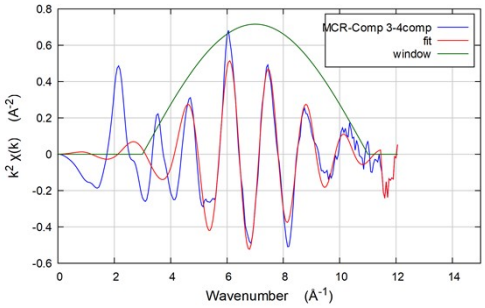

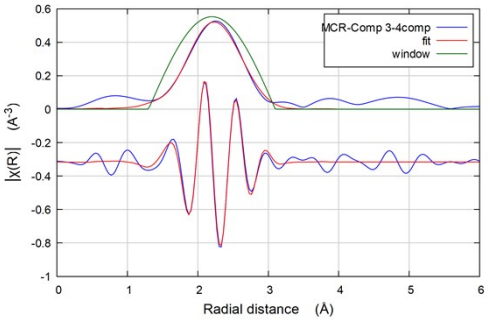

Comp 4

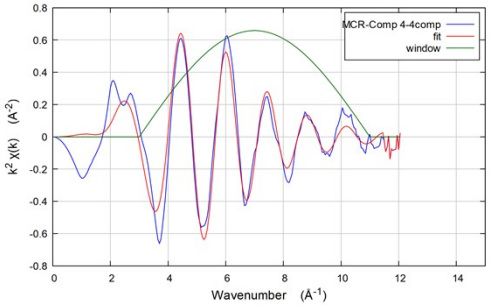

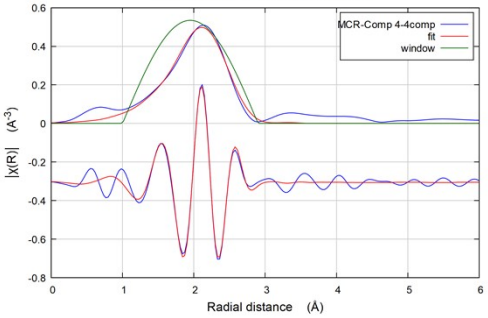

Fig SI 17. Fits of the EXAFS portion of the 4 MCR-ALS pure components obtained by the analysis of the dataset collected during the experiment with the low voltage cut-off at 0.01 V: EXAFS signal (left) and Fourier Transform (right).

Table S2. Fitting parameters of the EXAFS signal of the 5 MCR-ALS pure components obtained by the analysis of the dataset collected during the experiment with the low voltage cut-off at 0.01 V.

Component	Shell	S_0^2	N	R (theory)	R (fitted)	σ^2
Comp 1	Mn-P	0.50	6	2.25	2.284(8)	0.0076(4)
	Mn-Mn		1	2.95	2.69(1)	0.003(1)
	Mn-Mn		1	3.75	3.63(2)	0.002(2)
	Mn-P		10	3.90	3.92(3)	0.025(5)
Comp 2	Mn-P	0.50	6	2.25	2.285(8)	0.0079(4)
	Mn-Mn		1	2.95	2.69(1)	0.002(1)
	Mn-Mn		1	3.75	3.64(2)	0.003(2)
	Mn-P		10	3.90	3.92(4)	0.027(6)
Comp 3	Mn-Mn	0.50	4 (8)	2.668	2.59(2)	0.0096(6)
	Mn-Mn		3 (6)	3.081	2.98(2)	0.0096(6)
Comp 4	Mn-P	0.50	6	2.30	2.29(5)	0.023(3)
	Mn-Mn		1	2.73	2.67(2)	0.013(1)